Dalton Transactions

ROYAL SOCIETY OF CHEMISTRY

PAPER

View Article Online
View Journal | View Issue

Check for updates

Cite this: *Dalton Trans.*, 2026, **55**, 3776

Investigations of Co(II) to Co(III) oxidation mechanisms at $Fe_{3-\delta}O_4$ nanoparticle surfaces

Laura Fablet,[a,b] Mathieu Pédrot, [a] Fadi Choueikani,[b] Anthony Beauvois, [b] Thomas Stephant,[c] Valérie Briois[d] and Rémi Marsac *[e]

Received 18th December 2025,
Accepted 31st January 2026

DOI: 10.1039/d5dt03034j

rsc.li/dalton

Understanding and predicting the interaction mechanisms between Co and spinel iron oxides ($Fe_{3-\delta}O_4$), including magnetite, maghemite and their solid solutions, is of major interest in both the environmental and industrial contexts. While the surface complexation of Co^{2+}, its polymerization and the surface precipitation of $Fe_{3-\delta}O_4$@CoO have been well documented, the oxidation of Co^{2+} to Co^{3+} and interaction mechanisms between Co^{3+} and $Fe_{3-\delta}O_4$ nanoparticles in the presence of O_2 have attracted less attention. In this study, experimental and modeling results, combined with XAS and XMCD analyses at the $L_{2,3}$-edges, as well as TEM and XRD analysis, enabled the differentiation of several Co species according to the Co concentration, at pH 8 under atmospheric O_2. At the lowest Co concentrations investigated, Co^{2+} prevailed as surface complexes, incorporated into $Fe_{3-\delta}O_4$ nanoparticles, or as $Co(OH)_2$-like surface precipitates. Increasing the Co concentration led to the formation of an additional Co_3O_4-like phase on the surface of $Fe_{3-\delta}O_4$ nanoparticles. Quick-XAS measurements at the Co K-edge allowed the kinetics of Co sorption and oxidation on $Fe_{3-\delta}O_4$ nanoparticles to be followed, supporting the equilibrium observations. These results provide a more detailed understanding of mechanisms for Co sorption onto $Fe_{3-\delta}O_4$ nanoparticles under oxic conditions, which offers an alternative environmentally friendly route for the synthesis of Co-doped $Fe_{3-\delta}O_4$ nanoparticles. In addition, this enables understanding of the potential interactions between Co and $Fe_{3-\delta}O_4$ nanoparticles in environmental systems.

Published on 02 February 2026. Downloaded by INIST-CNRS - (Physics) on 3/27/2026 2:38:31 PM.

1. Introduction

Cobalt (Co) forms compounds with magnetic and electronic properties[1,2] that are of interest for many applications, including nanosensors, nanoelectronic devices and catalysts.[3,4] It occurs mainly in two oxidation states: Co^{2+} and Co^{3+}.[5–7] Co oxides also occur in the environment, with Co(II) (hydr)oxides (CoO, $Co(OH)_2$) and mixed Co(II,III) oxides (Co_3O_4), the latter being the most stable oxide form.[8,9] Co_3O_4 nanoparticles are the most extensively studied because, unlike CoO and $Co(OH)_2$, Co_3O_4 is an interesting candidate as a substitute for noble metals in electronic devices, being a stable semiconductor under ambient conditions.[3,10] Co_3O_4 has a spinel structure, with octahedral sites occupied by Co(III) ions and tetrahedral sites occupied by Co(II) ions.[4,9,11] Additionally, it can act as an effective catalyst for environmental remediation,[12] and also exhibits promise for the adsorption of organic pollutants.[13]

Co is often combined with oxides to form nanocomposites or core–shell particles, thereby improving physicochemical properties. Co is particularly studied in the presence of spinel iron oxides ($Fe_{3-\delta}O_4$) for the synthesis of cobalt ferrite particles or $Fe_{3-\delta}O_4$@Co(II)-(hydr)oxide particles composed of a magnetite/maghemite core and a Co oxide or Co ferrite shell.[14] Magnetite has an inverse spinel structure, in which Fe(II) occupies octahedral sites and Fe(III) occupies both octahedral and tetrahedral sites.[15–16] The stoichiometry of magnetite is defined by the Fe(II)-to-Fe(III) ratio (R), which ranges from 0.5, corresponding to fully stoichiometric magnetite ($\delta = 0$), to 0, where the magnetite structure is close to that of maghemite ($\delta = \frac{1}{3}$, Fe_2O_3).[17] This stoichiometry depends on various environmental factors (pH, microbial activity, organic ligands),[18–20] and the Fe(II) present in the structure can also be easily oxidized to Fe(III) in the presence of O_2.[17,21] Nevertheless, a small fraction of Fe(II) is resistant to oxidation and can persist for several years, even under acidic conditions such as pH 4, corresponding to $R = 0.1$.[22] Similarly, while Co(II) is stable at the magnetite surface under anaerobic conditions, partial oxidation of Co(II) to Co(III) has been reported under oxic conditions, leading to the formation of Co_3O_4 precipitates on the surface of maghemite.[23]

[a]*Univ Rennes, CNRS, Géosciences Rennes – UMR 6118, F-35000 Rennes, France*
[b]*Synchrotron SOLEIL, l'Orme des Merisiers, Départementale 128, 91190 Saint-Aubin, France*
[c]*Univ Rennes, CNRS, ISCR – UMR 6226, F-35000 Rennes, France*
[d]*Synchrotron SOLEIL, UR1-CNRS, France*
[e]*Université Paris Cité, Institut de physique du globe de Paris, CNRS, F-75005 Paris, France. E-mail: remi.marsac@cnrs.fr*

This journal is © The Royal Society of Chemistry 2026

Published on 02 February 2026. Downloaded by INIST-CNRS - (Physics) on 3/27/2026 2:38:31 PM.

The majority of magnetite@Co-(hydr)oxide syntheses are carried out in organic solvents or at high temperatures.[1,24,25] In contrast, the mechanisms controlling the oxidation of Co(II) to Co(III) at the magnetite surface have been only rarely characterized in aqueous solutions, even though such studies could support the development of more environmentally friendly synthesis procedures or reflect environmentally relevant processes. Schenck *et al.* (1983) showed that Co exists as a mixture of Co(II) and Co(III) on the surface of goethite particles at pH values above 8 in the presence of atmospheric O_2.[26] Conversely, other studies have demonstrated that at low Co concentrations, Co(II) remains stable at the surface of magnetite and forms structures close to that of Co ferrite.[23,27–29] Comparable concentration-dependent oxidative precipitation processes have been observed for other metal ions. For example, Ce(III) was shown to oxidize to Ce(IV) and precipitate at the goethite surface.[30] This oxidation process was favored at high [Ce]. Another example is the oxidation of Mn(II) on the surface of lepidocrocite, leading to the formation of Mn(III,IV) precipitates, where the extent of precipitation increases with pH and level of initial Mn(II) concentration.[31] Therefore, the speciation of Co on Fe oxides, and the potential formation of $Fe_{3-\delta}O_4$@Co(II,III)-(hydr)oxide, may be strongly influenced by the prevailing physicochemical conditions.

However, there remains a significant lack of information on whether environmentally friendly syntheses of such core@shell particles based on Co-decorated magnetite can be achieved under oxidizing conditions and also insufficient knowledge about the oxidation mechanisms of Co at iron oxide surfaces as well as the nature of the species formed. The present study investigated the sorption of Co onto oxidized magnetite nanoparticles ($Fe_{3-\delta}O_4$, non-stoichiometric magnetite, in which a small amount of Fe(II) was previously shown to persist, with R = 0.1) in aqueous suspensions.[22,23] The objectives were to (i) elucidate the surface speciation of Co on magnetite under various conditions in the presence of atmospheric O_2 and (ii) understand the kinetics of Co sorption at the surface of $Fe_{3-\delta}O_4$. Adsorption experiments were conducted, and the surface speciation of Co was investigated using X-ray absorption spectroscopy (XAS) and magnetic circular dichroism (XMCD) at the $L_{2,3}$-edges, as well as TEM and XRD analyses. The kinetics of Co sorption at the $Fe_{3-\delta}O_4$ surface was monitored using quick-XAS at the Co K-edge. The results provide valuable insights into the environmentally friendly synthesis of core@shell particles with an $Fe_{3-\delta}O_4$ core and a Co-based shell in aqueous solution under oxic conditions, and contribute to a better understanding of Co behavior and fate in the environment.

2. Materials and methods

2.1. Chemicals

All chemicals used were purchased from Sigma-Aldrich and were of analytical grade or better. Sample solutions were prepared with "MilliQ" ultrapure water (specific resistivity of 18.2 MΩ cm). For microscopy measurements, hexadecyltrimethylammonium bromide (CTAB) was used as a surfactant. The Co hydroxide and Co ferrite references used were synthesized in a previous study.[23,29]

2.2. Synthesis of $Fe_{3-\delta}O_4$ nanoparticles and reference Co samples

Stoichiometric magnetite nanoparticles were synthesized at room temperature in an anaerobic chamber (N_2-glovebox, JACOMEX, $O_{2(g)}$ < 1 ppm) by coprecipitation of iron salts.[17,22,32] The dissolution of $FeCl_2$ and $FeCl_3$ in HCl solution, followed by addition of this solution to NaOH solution, led to the instantaneous precipitation of ~10 nm magnetite nanoparticles.[17] To obtain oxidized magnetite, H_2O_2 was added in excess to decrease the stoichiometry of the magnetite as much as possible. The synthesized nanoparticles were washed with ultrapure water adjusted to pH ~ 8.5 (using NaOH) to prevent the release of Fe^{2+}. The stoichiometry of the synthesized $Fe_{3-\delta}O_4$ nanoparticles was verified by spectrophotometric determination of the dissolved [Fe(II)] and total [Fe] (*i.e.* [Fe(III)] + [Fe(II)]) using the 1,10-phenanthroline colorimetric method.[33,34] The $R_{0.1}$ sample was taken out of the anaerobic chamber immediately before use.

A cobalt ferrite suspension was prepared using the same procedure as that for stoichiometric magnetite, but replacing 10% of the Fe(II) with Co(II) ($CoCl_2{\cdot}6H_2O$). A cobalt hydroxide suspension was prepared from 100 mM $CoCl_2$ stock solution, which was neutralized by adding NaOH until precipitation occurred. The solution was then stabilized at pH 10 by adding NaOH.

2.3. Sorption experiments

Aqueous suspensions of $Fe_{3-\delta}O_4$ nanoparticles ($R_{0.1}$) were prepared at a total Fe concentration of 13 mM (equivalent to 1 g L^{-1} magnetite) in 50 mL polypropylene tubes, containing 10 mM NaCl. Sorption isotherm experiments were performed at pH 8 using varying total Co concentrations ($[Co]_{tot}$) prepared from a 100 mM $CoCl_2$ stock solution ($[Co]_{tot}$ = 0.1, 0.5, 1.0, 2.0, 2.8, 3.8, 4.9, 5.9, 6.8, 7.8, 8.5, 9.4, 10.5 and 11.8 mM). Experiments were performed outside the anaerobic chamber, but $N_{2(g)}$ bubbling was used: this limits carbonate dissolution (which could otherwise lead to $CoCO_3$ complexation or precipitation) but cannot prevent $O_{2(g)}$ for the potential oxidation of Co(II) to Co(III). After 7 days of equilibration, a magnet was used to collect the solid fraction of the suspensions. The supernatant was filtered at 0.2 μm using cellulose PES filters (Sartorius Minisart). Solid-phase Co concentrations were determined using a UV-vis spectrophotometric method adapted from Zahir and Keshtkar (1998).[35] The method is based on complexation of Co^{2+} with 1-nitroso-2-naphthol-3,6-disulfonic acid disodium salt hydrate (nitroso-R salt). The absorbance was recorded at 520 nm with a Shimadzu UV2600 spectrophotometer. The total amount of Co associated with the solid phase was expressed in terms of the Co surface density on $Fe_{3-\delta}O_4$ ($[Co]_s$ in atoms per nm^2) and calculated as follows:

$$[Co]_s = ([Co]_{tot} - [Co]_{aq}) \times \frac{V}{m} \times \frac{1}{SSA} \times N_A \times 10^{-18} \quad (1)$$

Published on 02 February 2026. Downloaded by INIST-CNRS - (Physics) on 3/27/2026 2:38:31 PM.

where $[Co]_{tot}$ and $[Co]_{aq}$ are given in mol L^{-1}, V is the sample volume (L), m is the $Fe_{3-\delta}O_4$ mass (g), SSA is the specific surface area ($m^2\ g^{-1}$) and N_A is the Avogadro constant (mol^{-1}).

2.4. Characterization by TEM and XRD

Non-stoichiometric magnetite nanoparticles were characterized by high-resolution transmission electron microscopy (HR-TEM, Jeol JEM 2100 HR microscope) for four Co concentrations ($[Co]_{tot}$ = 0.5, 3, 6 and 12 mM). A small volume of sample was taken and diluted with ultrapure water. All samples were sonicated for 15 min. A droplet of the diluted suspension was then deposited on a holey-carbon 300-mesh copper grid and dried under ambient conditions.

Two samples ($[Co]_{tot}$ = 2 and 12 mM) were analyzed by powder X-ray diffraction (XRD) using a Bruker D8 Advance diffractometer equipped with monochromatized Cu Kα1 radiation (λ = 0.15406 nm). The energy window of the LynxEye detector was adjusted in order to suppress fluorescence background from Fe and Co atoms. The Co-$Fe_{3-\delta}O_4$ solid phases were separated from solution using a magnet, then deposited and dried on a disoriented Si single-crystal holder.

2.5. XAS and XMCD analysis at Co and Fe $L_{2,3}$-edges

Solid samples were analyzed by XAS and XMCD, covering the soft X-ray range and probing the $L_{2,3}$ (2p → 3d) absorption edges of the Fe and Co transition metals. The chemical selectivity and sensitivity to valence states of XAS and XMCD at $L_{2,3}$-edges allows us to better understand the contribution made by the Co and Fe cations to the structure and magnetic behavior of the nanoparticles. XAS and XMCD spectra were recorded on the DEIMOS beamline at Synchrotron SOLEIL.[36] Measurements were carried out on dried nanoparticles by dropping colloidal suspensions on silicon plates previously dried at room temperature. Then, the silicon plates were fixed to a copper sample holder, which was then introduced into the superconducting magnet of the DEIMOS end station. All spectra were collected in total electron yield (TEY) mode at 4.2 K and under UHV conditions (10^{-10} mbar). XAS spectra were recorded by reversing the full circular polarization of the X-rays to the right (σ_R) or left (σ_L), and by varying the external magnetic field (H = +6 or −6 T). Isotropic XAS spectra were plotted as $(\sigma^+ + \sigma^-)/2$, while the XMCD results were plotted as $(\sigma^+ - \sigma^-)$, where $\sigma^+ = [\sigma_L(H^-) + \sigma_R(H^+)]/2$ and $\sigma^- = [\sigma_L(H^+) + \sigma_R(H^-)]/2$. For all Co spectra, the XAS and XMCD background at Co $L_{2,3}$-edges was deleted using OriginPro software. XAS and XMCD were normalized by dividing the raw signal by the edge jump of the isotropic XAS. At the DEIMOS beamline, the XAS and XMCD measurements require an Apple-II HU52 undulator to produce the fully circularly polarized X-rays. The beam size was 800 × 800 μm^2 and the photon energy resolution was 100 meV.

2.6. Quick-XAS analysis at the Co and Fe K-edges

Cobalt adsorption and oxidation kinetics were monitored by quick-EXAFS at the ROCK beamline of Synchrotron SOLEIL.[37] Quick-XAS spectra were acquired at the Fe and Co K-edges using a Si(111) channel-cut monochromator set at 15.3° with an oscillation amplitude of 3.0°, allowing both edges to be recorded within the same energy scan. Harmonic rejection was achieved using two B_4C-coated mirrors (positioned before and after the monochromator) aligned at 2.8 mrad relative to the X-ray beam. The channel-cut oscillated at 2 Hz, yielding one spectrum every 250 ms. A compromise between time resolution and signal-to-noise ratio was obtained by merging consecutive spectra over 50 s. Measurements were performed in fluorescence mode using a passivated implanted planar silicon detector (Canberra, Inc.)

The kinetic experiments were performed using a cell developed at the ROCK beamline,[38] which allows chemical kinetics in the liquid phase under stirring to be monitored. An aliquot of Co(II) solution was added to a suspension of $Fe_{3-\delta}O_4$ nanoparticles, under ambient air conditions with Ar bubbling, to obtain a final suspension volume of 100 mL at an initial pH ∼ 6. The experiment was performed for $[Co]_{tot}$ = 12 mM with a fixed final Fe concentration ($[Fe]_{tot}$ = 13 mM). An automatic titrator (Titrino Metrohm) was operated in SET mode to raise and then maintain the pH at 8, using a 1 M NaOH solution. The use of concentrated NaOH limited dilution of the samples. The titrator was started 10 min after injection of Co into the $Fe_{3-\delta}O_4$ nanoparticle suspension.

Spectra were processed and energy-aligned using the extract_gui and normal_gui Python graphical interfaces developed at the ROCK beamline.[38] The energy alignment of the Fe and Co K-edge spectra was performed using monochromator glitches that had been absolutely calibrated by setting the first inflection point of Fe and Co foil XAS spectra to 7112 eV and 7709 eV, respectively. The quick-XAS dataset was analyzed by principal component analysis (PCA), multivariate curve resolution with alternating least squares (MCR-ALS), and linear combination fitting (LCF) implemented in the FASTOSH software.[39]

2.7. Chemical speciation modelling

Aqueous chemical speciation calculations were performed using PhreePlot.[40] The "Minteq.v4.dat" database was used for the calculations. Ionic strength effects on equilibrium constants were evaluated using the Davies equation.

3. Results and discussion

3.1. Effects of cobalt concentration on its oxidation at $Fe_{3-\delta}O_4$

To determine the surface speciation of Co, XAS and XMCD spectra at the Fe and Co $L_{2,3}$-edges were recorded for various Co concentrations ($[Co]_{tot}$ = 0.5 to 12 mM), at pH 8. The corresponding values for the concentration of total Co, solid-phase Co and dissolved Co are given in Table S1. The Co L_3-edge XAS spectra are presented in Fig. 1a. At low Co concentrations, when $[Co]_s \leq 2.47$ atoms per nm^2, the XAS spectra are typical of Co^{2+}, with four contributions at 780.7 eV (peak A), 781.8 eV (peak B), 782.4 eV (peak C), and 783.1 eV (peak D), corres-

 This journal is © The Royal Society of Chemistry 2026

Published on 02 February 2026. Downloaded by INIST-CNRS - (Physics) on 3/27/2026 2:38:31 PM.

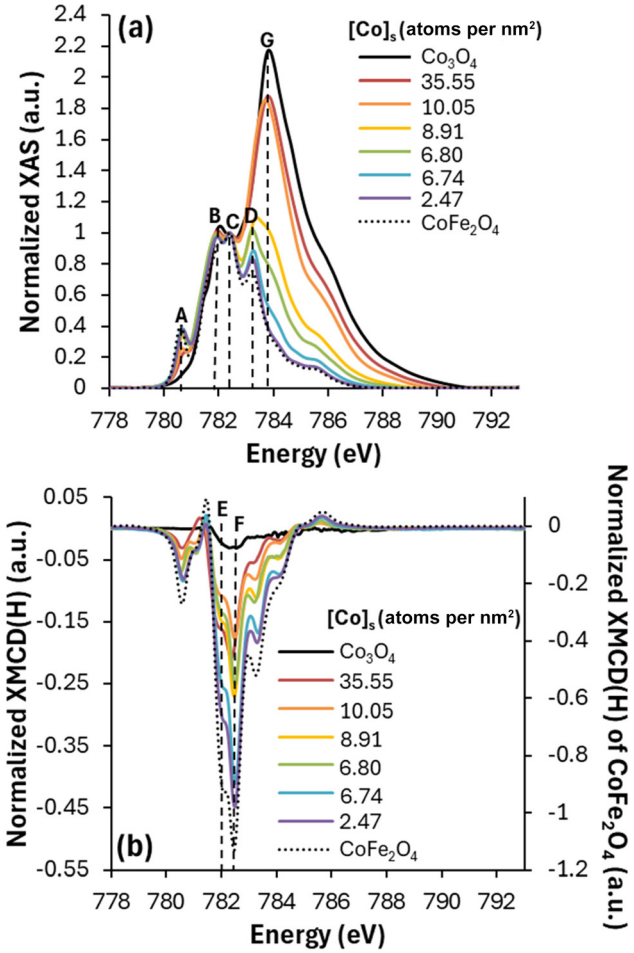

Fig. 1 Normalized isotropic XAS (a) and XMCD (b) spectra at the Co L_3-edge of Co adsorbed onto $Fe_{3-\delta}O_4$ at pH 8 with different $[Co]_{tot}$ values (from 2.47 to 35.55 atoms per nm^2). The dotted line corresponds to the $CoFe_2O_4$ reference spectrum, and the black line to the Co_3O_4 reference (data from Fablet *et al.*, 2024).[23] XAS spectra are normalized to the C peak, and XMCD signals are normalized by dividing the raw signal by the edge jump of XAS. Note that the XMCD spectrum of $CoFe_2O_4$ corresponds to the secondary *y*-axis.

ponding to multiplet splitting typical of Co^{2+}.[41] All XAS spectra were normalized to peak C to facilitate comparison of the relative intensities of the other peaks. At this concentration, the XAS spectrum is similar to that of the $CoFe_2O_4$ reference, suggesting adsorption, incorporation or formation of small oligomers of Co onto the $Fe_{3-\delta}O_4$ surface, as they cannot be distinguished on the basis of soft XAS analysis only.[23,29] The presence of $Co(OH)_2$ cannot be excluded, showing the same multiplet peaks A, B, C and D, but with a more intense B peak signal.[23,29,42] When the Co concentrations are increased, when $[Co]_s$ = 6.80 and 8.91 atoms per nm^2, a shoulder emerges at a higher energy than that for peak D, corresponding to a small peak G at 783.8 eV. Finally, for high Co concentrations ($[Co]_s$ = 10.05 and 35.55 atoms per nm^2), the spectra exhibit a diminished peak A signal and a prominent peak G signal. These spectral features are consistent with those of Co_3O_4, a mixed-valence compound containing both Co(II) and Co(III), which typically shows an intense peak G but lacks a peak A signal.

These results indicate the formation and progressive development of a Co_3O_4-like phase with increasing Co concentration. As demonstrated in a previous study,[23] Co(II) can be partially oxidized to Co(III) at pH 8 under ambient atmospheric conditions and at room temperature, leading to the formation of a Co_3O_4-like phase on the particle surface. The XMCD spectra, presented in Fig. 1b, exhibit two peaks at 782.2 eV (peak E) and 782.5 eV (peak F), which are characteristic of Co^{2+}. The XMCD signal for all concentrations is negative, indicating that Co^{2+} occupies octahedral sites. At low Co concentration, the XMCD signal intensity is lower than that of the $CoFe_2O_4$ reference, but similar to the signal previously obtained under anaerobic conditions at the same solid-phase Co concentration.[23] This confirms the presence of Co-oligomeric species on the $Fe_{3-\delta}O_4$ surface. A decrease in the XMCD signal is observed when $[Co]_{tot}$ increases, also suggesting the formation and growth of a Co_3O_4-like phase, which does not contribute to the XMCD signal. Regardless of the $[Co]_s$ studied, XAS and XMCD analyses at Fe $L_{2,3}$-edges (Fig. S1) showed no detectable effect of Co on the stoichiometry of magnetite, which remains at around R = 0.1. TEM images are shown in Fig. S2 for four Co concentrations ($[Co]_s$ = 2.47, 6.80, 10.05 and 35.55 atoms per nm^2). Nanoparticles are highly aggregated, consistent with the observation by Fablet *et al.* (2024),[23] although the degree of aggregation appears to increase with Co concentrations. At $[Co]_s \geq 6.80$ atoms per nm^2, a few Co-rich crystalline sheets were observed, probably corresponding to distinct precipitated Co_3O_4-like nanoparticles, as confirmed by energy-dispersive X-ray spectroscopy (Fig. S3).

To confirm the composition of samples, XRD analysis was performed for $[Co]_s$ = 6.74 atoms per nm, which contains only Co(II)-bearing phases, and for $[Co]_s$ = 35.55 atoms per nm^-, for which a Co_3O_4 phase was indicated by $L_{2,3}$-edge XAS results (Fig. 2). Both of these XRD patterns exhibit the large peak characteristics of nanocrystallized phases. The theoretical patterns of Fe_3O_4,[43] $CoFe_2O_4$,[44] Co_3O_4 [45] and $Co(OH)_2$ [46] have been simulated using the Rietveld method. For $CoFe_2O_4$, a $MgAl_2O_4$-type spinel structure was assumed, implying the Co^{2+} was in an octahedral position to best fit the XRD data. The sample with $[Co]_s$ = 6.74 atoms per nm^2 is fully indexed with the theoretical $CoFe_2O_4$ pattern, with a unit cell parameter of a = 8.362 Å. This parameter is not significantly smaller than the one for Fe_3O_4 (a = 8.397 Å). The presence of $Co(OH)_2$ was not detected in the XRD patterns. However, previous TEM observations revealed the formation of an amorphous $Co(OH)_2$ phase precipitated on the surface of magnetite nanoparticles, under anaerobic conditions,[29] which could not be detected by XRD. Therefore, the presence of amorphous $Co(OH)_2$ cannot be excluded. For $[Co]_s$ = 35.55 atoms per nm^2, the XRD pattern shows the presence of the same phase with similar unit cell parameters. Furthermore, two sets of additional peaks appear. The first set, with the broad peak characteristics of a nanocrystalline phase, is shifted to higher Bragg angles compared to

Published on 02 February 2026. Downloaded by INIST-CNRS - (Physics) on 3/27/2026 2:38:31 PM.

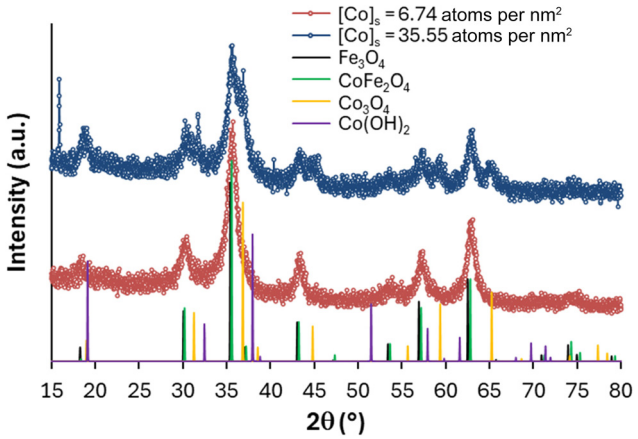

Fig. 2 X-ray diffraction (XRD) patterns of the $Fe_{3-\delta}O_4$ samples with $[Co]_s$ = 6.74 (blue) and 35.55 atoms per nm^2 (red), and theoretical patterns of Fe_3O_4 (black),[43] $CoFe_2O_4$ (green),[44] Co_3O_4 (yellow),[45] and $Co(OH)_2$ (purple).[46]

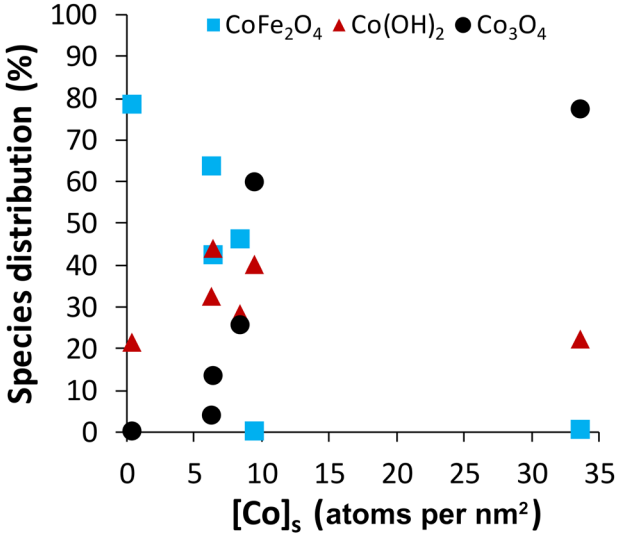

Fig. 3 Co surface speciation determined by LCF of the Co L_3-edge XAS spectra using $CoFe_2O_4$, $Co(OH)_2$ and Co_3O_4 as reference compounds.

the peak for Fe_3O_4 or $CoFe_2O_4$, corresponding to the Co_3O_4 spinel phase (a = 8.082 Å). The second set, with thin diffraction peaks at 15.9° and 31.7°, probably arises from the crystallization of residual salts (*e.g.* NaCl and/or hydrated salts) during powder drying. These XRD results confirm the absence of a Co_3O_4 phase with low Co concentration, and the coexistence of a $CoFe_2O_4$-type phase and a Co_3O_4 precipitate at high Co concentrations.

Linear-combination analyses of the normalized Co L_3-edge XAS spectra (from 775.5 to 804.5 eV) were performed to estimate the Co surface speciation as a function of $[Co]_s$, using three reference compounds: $Co(OH)_2$, $CoFe_2O_4$ and Co_3O_4 (Fig. 3 and Fig. S4, Table S2). In agreement with previous studies conducted under anaerobic conditions, $CoFe_2O_4$-like species dominate at low [Co], but their proportion decreases with increasing $[Co]_s$ in favor of a $Co(OH)_2$-like phase.[23,29] Co_3O_4 does not form for [Co] < 6 atoms per nm^2, but accounts for more than 60% when [Co] > 10 atoms per nm^2. Interestingly, a significant fraction of the $Co(OH)_2$-like phase (~20%) persists even at very high surface loadings, although equilibrium calculations (pH–E_H predominance diagram for Co in Fig. S5) predict complete transformation to Co_3O_4 under these conditions.

3.2. Effects of pH on Co oxidation at $Fe_{3-\delta}O_4$

As the L_3-edge XAS spectra indicate similar amounts of the Co_3O_4-like phase between $[Co]_{tot}$ = 6 and 12 mM ($[Co]_s$ = 10.05 and 35.55 atoms per nm^2, respectively), the effect of the increase of pH to 10 on Co sorption at $Fe_{3-\delta}O_4$ was investigated for $[Co]_{tot}$ = 6 mM. According to the pH–E_H predominance diagram for Co (Fig. S5), Co_3O_4 is expected to be more stable at pH 10. Sorption experiments revealed 97% Co adsorption at pH 10, corresponding to a surface loading of 29.68 atoms per nm^2. The Co L_3-edge XAS spectra at pH 8 and 10 are presented in Fig. 4. At pH 10, the XAS spectrum shows a slightly more intense G peak than at pH 8, in qualitative agreement with

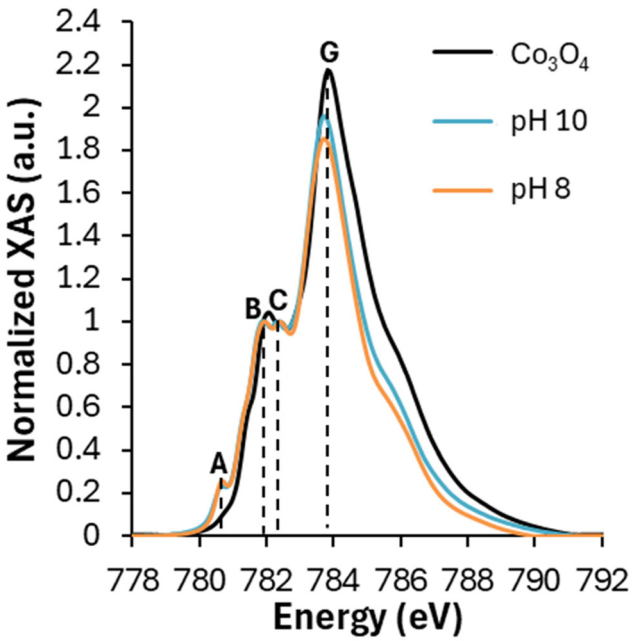

Fig. 4 Normalized isotopic XAS spectra at the Co L_3-edge of Co adsorbed onto $Fe_{3-\delta}O_4$ at pH 8 (orange) and pH 10 (blue) for $[Co]_{tot}$ = 6 mM. XAS spectra are normalized to peak C.

thermodynamic calculations. However, its intensity remains ~10% lower than that of the Co_3O_4 reference, therefore suggesting an incomplete oxidation process under the present experimental conditions. Alternatively, the Co_3O_4-like phase formed at the surface of $Fe_{3-\delta}O_4$ might differ structurally from the crystallized Co_3O_4 reference, which might explain the observed spectral differences.

This journal is © The Royal Society of Chemistry 2026

Published on 02 February 2026. Downloaded by INIST-CNRS - (Physics) on 3/27/2026 2:38:31 PM.

3.3. Oxidation mechanisms

To understand the Co oxidation mechanism at the surface of $Fe_{3-\delta}O_4$, time-resolved quick-XAS analyses were performed at both the Co and Fe K-edges. The XANES spectra collected during the oxidation experiment of Co are presented in Fig. 5 for $[Co]_{tot}$ = 12 mM (corresponding to 35.55 atoms per nm^2). The sample was analyzed for approximately 10 min at the initial pH (~6) to characterize the first component (red spectra), which corresponds mainly to aqueous Co^{2+} due to the weak Co(II) adsorption at this pH (black spectrum) (Fig. S6).[23] After ~10 min of analysis, the pH is raised to 8 using NaOH. The target pH is reached after 18.5 min, during which time spectra evolution is observed. The end of this step corresponds to the black spectrum in Fig. 5. Subsequently, while maintaining the pH at 8, the spectra continue to evolve (red to blue spectra in Fig. 5), although to a lesser extent during the final minutes of the experiments. The position of the white line (WL) shifts from 7725.4 eV (at the beginning of the experiment) to 7728.4 eV (at the end), and the concurrent decrease in WL intensity indicates oxidation of Co(II) to Co(III).[47] The presence of a pre-edge at 7710.0 eV can be noted, which is a characteristic of distorted octahedral environments in transition metal oxides. This pre-edge peak has a lower intensity than that derived from tetrahedral environments,[48,49] which is in agreement with the XAS and XMCD analyses at Co $L_{2,3}$-edges that reveal no Co species are present in the tetrahedral environment. For example, the presence of this pre-peak is found in spectra of Co ferrite[50] or Co oxide, corresponding to the presence of Co(II) within octahedral sites.[51] The kinetics at the Fe K-edge (Fig. S7) shows no modification of the XAS spectra, highlighting that Fe species do not evolve during the kinetics, and that the oxidation state of Fe in particular does not change, hence suggesting that $O_{2(g)}$ rather than Fe(III) acts as a redox partner.

From the XAS spectra, MCR-ALS analyses were carried out. Preliminary PCA indicated that three components were required to describe the variance in the spectral data matrix (Fig. S8). The concentration profiles of the extracted components as a function of pH evolution are shown in Fig. 6a. The proportion of the first component decreases as the pH increases, and persists until t = 104 min, before disappearing. The second component forms from t = 8 min when the pH begins to increase. The maximum of the second component is reached at pH = 6.4 (75.6%). This component persists until t > 110 min. Finally, the third component appears at t = 14 min, and increases until t > 110 min, when the pH is stable. The XANES spectra of the pure components obtained from the MCR-ALS analysis are shown in Fig. 6b, and compared to the $Co^{2+}{}_{aq}$, $Co(OH)_2$, $CoFe_2O_4$ and Co_3O_4 references. As mentioned, before, the XANES spectrum of component 1 is characteristic of the spectrum of the Co^{2+} hexa-hydrated reference with a maximum intensity of the WL at 7725.4 eV (Fig. S6), which is the typical position of the WL in Co^{2+} samples found in the literature.[52,53] With respect to component 2, the WL of the XANES spectrum exhibits an intense feature comparable to that of the $CoFe_2O_4$ spectrum at 7727.5 eV, which is characteristic of an element positioned within an octahedral unit of a spinel structure.[54,55] However, the spectrum also has a shoulder at 7724.8 eV, suggesting the presence of $Co(OH)_2$. The maximum intensity of the WL of the XANES spectrum of component 3 is found at 7728.7 eV, which is an intermediate energy value between that of $CoFe_2O_4$ at 7727.5 eV and that of Co_3O_4 at 7729.3 eV, suggesting the presence of Co(II) and Co(III) in the structure of the nanoparticles. It is possible that a $Co(OH)_2$ phase is also present due to the width of the WL. Therefore, time-resolved analysis confirms the slow oxidation of Co(II) phases into Co_3O_4, with the persistence of $CoFe_2O_4$/$Co(OH)_2$, which was also observed after longer reaction times by conducting soft XAS analysis.

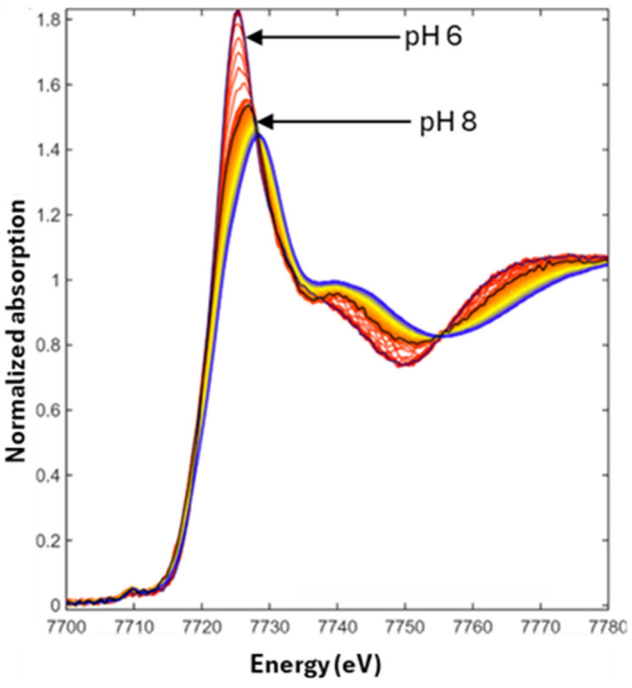

Fig. 5 XANES spectra evolution at the Co K-edge as a function of time (0–120 min, from red to blue) during the oxidation kinetics under aerobic conditions for $[Co]_{tot}$ = 12 mM. The samples were analyzed for approximately 10 min at the initial pH (~6), then the pH was raised to 8 using NaOH. The black spectrum was recorded when pH 8 was reached.

4. Conclusion

Co nanoparticles are widely used in many high-tech applications, including the synthesis of nanocomposites and core–shell particles. The affinity of Co for Fe-oxide nanoparticles, particularly spinel Fe oxides (magnetite and maghemite), facilitates the synthesis of hybrid particles with great potential due to their unique resulting properties. However, the interactions between $Fe_{3-\delta}O_4$ nanoparticles and Co remained insufficiently understood. This study investigates the mechanisms governing these interactions under oxic conditions. XAS and XMCD analyses at the $L_{2,3}$-edges revealed several distinct

Published on 02 February 2026. Downloaded by INIST-CNRS - (Physics) on 3/27/2026 2:38:31 PM.

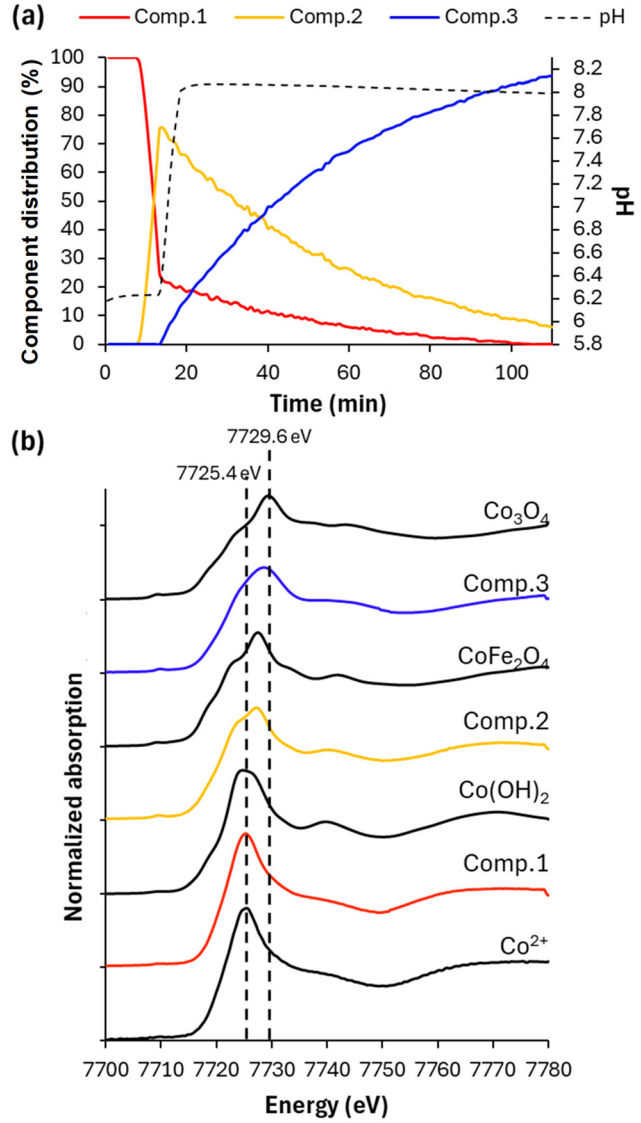

Fig. 6 (a) Concentration profiles as a function of time of three components extracted by MCR-ALS analysis. The secondary axis shows the pH evolution (dotted line) from pH ~6 to ~8. (b) XANES spectra of components 1, 2 and 3. Black spectra correspond to the references of Co^{2+}, $Co(OH)_2$, $CoFe_2O_4$ and Co_3O_4.

behaviors depending on Co concentration. At low Co concentrations, Co forms a mixture composed of $CoFe_2O_4$-like and $Co(OH)_2$-like phases. As the Co concentration increases, a third species is formed, corresponding to a Co_3O_4-like phase. To further elucidate Co sorption and oxidation dynamics, Co sorption kinetics on $Fe_{3-\delta}O_4$ was monitored by quick-XAS at the Co K-edge. The results showed that at pH ≤ 6, Co remains predominantly as Co^{2+} in solution. As pH increases, Co adsorbs onto the $Fe_{3-\delta}O_4$ surface, leading to its incorporation into a $CoFe_2O_4$-like structure and/or formation of a $Co(OH)_2$-like phase. Over time, surface-bound Co(II) partially oxidizes to form a Co_3O_4-like phase, as supported by XRD results, with limited formation of distinct Co-containing particles, as shown by TEM. These results highlight the ability of $Fe_{3-\delta}O_4$ nanoparticles to promote Co oxidation at room temperature under oxic conditions. These findings provide new insights into Co surface speciation as a function of concentration, pH, and reaction time. The possibility of forming $Fe_{3-\delta}O_4$@Co(II, III)-oxide particles under environmentally friendly synthesis conditions opens promising perspectives for high-tech applications.

Author contributions

Laura Fablet: writing – original draft, data curation, investigation, visualization. Mathieu Pédrot: writing – review & editing, resources, supervision, project administration, funding acquisition. Fadi Choueikani: writing – review & editing, resources, supervision, project administration, funding acquisition. Anthony Beauvois: writing – review & editing. Thomas Stephant: data curation, writing – review & editing. Valérie Briois: data curation, writing – review & editing. Rémi Marsac: writing – review & editing, resources, supervision, project administration, funding acquisition.

Conflicts of interest

There are no conflicts to declare.

Data availability

The data supporting this article have been included as part of the supplementary information (SI) and are available from the IPGP Research Collection (https://doi.org/10.18715/IPGP.2026.mkzt1as1). eText files contain raw Quick-XAS spectra at Co and Fe K-edge recorded every 50s, and reference spectra. Excel files contain (i) XAS and XMCD data at Co and Fe L2,3-edges and (ii) XRD data.

Supplementary information is available. See DOI: https://doi.org/10.1039/d5dt03034j.

Acknowledgements

This work was supported by the French Brittany Region (ARED project "NANOMAG"), SOLEIL synchrotron, and the "COLOSSAL" project funded by ANR (project number ANR-23-CE01-0001). Through the support of the GeOHeLiS analytical platform of Rennes University, this publication was also supported by the European Union through the European Regional Development Fund (FEDER), the French Ministry of Higher Education and Research, the French Region of Brittany and Rennes Metropole. The authors further acknowledge the SOLEIL synchrotron for beamtime allocation at the DEIMOS and ROCK beamlines (proposals no. 20210864 & 20230086). The work at ROCK was supported by a public grant overseen by the French National Research Agency (ANR) as part of the

This journal is © The Royal Society of Chemistry 2026

Published on 02 February 2026. Downloaded by INIST-CNRS - (Physics) on 3/27/2026 2:38:31 PM.

"Investissements d'Avenir" program (reference: ANR-10-EQPX-45). The authors are grateful to L. Dutruch and M. Pattier for assistance with ICP-MS and UV-vis analyses, and to V. Dorcet and L. Rault for assistance with TEM experiments performed on the THEMIS platform (ScanMAT, UMS 2011 University of Rennes-CNRS; CPER-FEDER 2007–2014).

References

1 K. Sartori, G. Cotin, C. Bouillet, V. Halté, S. Bégin-Colin, F. Choueikani and B. P. Pichon, Strong interfacial coupling through exchange interactions in soft/hard core–shell nanoparticles as a function of cationic distribution, *Nanoscale*, 2019, **11**, 12946–12958.

2 H. Zhang, Y. Liu and S. Sun, Synthesis and assembly of magnetic nanoparticles for information and energy storage applications, *Front. Phys. (China)*, 2010, **5**, 347–356.

3 S. Iravani and R. S. Varma, Sustainable synthesis of cobalt and cobalt oxide nanoparticles and their catalytic and biomedical applications, *Green Chem.*, 2020, **22**, 2643–2661.

4 J. Mei, T. Liao, G. A. Ayoko, J. Bell and Z. Sun, Cobalt oxide-based nanoarchitectures for electrochemical energy applications, *Prog. Mater. Sci.*, 2019, **103**, 596–677.

5 D.-H. Ha, L. M. Moreau, S. Honrao, R. G. Hennig and R. D. Robinson, The Oxidation of Cobalt Nanoparticles into Kirkendall-Hollowed CoO and Co_3O_4: The Diffusion Mechanisms and Atomic Structural Transformations, *J. Phys. Chem. C*, 2013, **117**, 14303–14312.

6 M. Martin, U. Koops and N. Lakshmi, Reactivity of solids studied by in situ XAS and XRD, *Solid State Ionics*, 2004, **172**, 357–363.

7 M. Verelst, T. O. Ely, C. Amiens, E. Snoeck, P. Lecante, A. Mosset, M. Respaud, J. M. Broto and B. Chaudret, Synthesis and Characterization of CoO, Co3O4, and Mixed Co/CoO Nanoparticules, *Chem. Mater.*, 1999, **11**, 2702–2708.

8 J. S. Choi and C. H. Yo, Study of the Nonstoichiometric Compositions of Cobaltous Oxide, *Inorg. Chem.*, 1974, **13**, 1720–1724.

9 A. Gulino, P. Dapporto, P. Rossi and I. Fragalà, A Novel Self-generating Liquid MOCVD Precursor for Co_3O_4 Thin Films, *Chem. Mater.*, 2003, **15**, 3748–3752.

10 M. Manickam, V. Ponnuswamy, C. Sankar and R. Suresh, Cobalt oxide thin films prepared by NSP technique: Impact of molar concentration on the structural, optical, morphological and electrical properties, *Optik*, 2016, **127**, 5278–5284.

11 A. F. Wells, *Structural Inorganic Chemistry*, OUP Oxford, 2012.

12 S. K. Jesudoss, J. J. Vijaya, P. I. Rajan, K. Kaviyarasu, M. Sivachidambaram, L. J. Kennedy, H. A. Al-Lohedan, R. Jothiramalingam and M. A. Munusamy, High performance multifunctional green Co304 spinel nanoparticles: photodegradation of textile dye effluents, catalytic hydrogenation of nitro-aromatics and antibacterial potential, *Photochem. Photobiol. Sci.*, 2017, **16**, 766–778.

13 A. Anele, S. Obare and J. Wei, Recent Trends and Advances of Co3O4 Nanoparticles in Environmental Remediation of Bacteria in Wastewater, *Nanomaterials*, 2022, **12**, 1129.

14 S. Jauhar, J. Kaur, A. Goyal and S. Singhal, Tuning the properties of cobalt ferrite: a road towards diverse applications, *RSC Adv.*, 2016, **6**, 97694–97719.

15 G. F. Goya, T. S. Berquó, F. C. Fonseca and M. P. Morales, Static and dynamic magnetic properties of spherical magnetite nanoparticles, *J. Appl. Phys.*, 2003, **94**, 3520–3528.

16 B. Issa, I. M. Obaidat, B. A. Albiss and Y. Haik, Magnetic Nanoparticles: Surface Effects and Properties Related to Biomedicine Applications, *Int. J. Mol. Sci.*, 2013, **14**, 21266–21305.

17 P. Jungcharoen, M. Pédrot, F. Choueikani, M. Pasturel, K. Hanna, F. Heberling, M. Tesfa and R. Marsac, Probing the effects of redox conditions and dissolved Fe 2+ on nanomagnetite stoichiometry by wet chemistry, XRD, XAS and XMCD, *Environ. Sci.: Nano*, 2021, **8**, 2098–2107.

18 J. M. Byrne, N. Klueglein, C. Pearce, K. M. Rosso, E. Appel and A. Kappler, Redox cycling of Fe(II) and Fe(III) in magnetite by Fe-metabolizing bacteria, *Science*, 2015, **347**, 1473–1476.

19 P. Jungcharoen, R. Marsac, F. Choueikani, D. Masson and M. Pédrot, Influence of organic ligands on the stoichiometry of magnetite nanoparticles, *Nanoscale Adv.*, 2023, **5**, 4213–4223.

20 A. Sundman, J. M. Byrne, I. Bauer, N. Menguy and A. Kappler, Interactions between magnetite and humic substances: redox reactions and dissolution processes, *Geochem. Trans.*, 2017, **18**, 6.

21 C. A. Gorski, J. Nurmi, P. Tratnyek, T. Hofstetter and M. M. Scherer, Redox Behavior of Magnetite: Implications for Contaminant Reduction, *Environ. Sci. Technol.*, 2010, **44**, 55–60.

22 P. Jungcharoen, M. Pédrot, F. Heberling, K. Hanna, F. Choueikani, C. Catrouillet, A. Dia and R. Marsac, Prediction of nanomagnetite stoichiometry (Fe(II)/Fe(III)) under contrasting pH and redox conditions, *Environ. Sci.: Nano*, 2022, **9**, 2363–2371.

23 L. Fablet, F. Choueikani, M. Pédrot and R. Marsac, What are the effects of environmental factors on Co speciation at the magnetite surface?, *Environ. Sci.: Nano*, 2024, **11**, 2036–2048.

24 T. Gaudisson, R. Sayed-Hassan, N. Yaacoub, G. Franceschin, S. Nowak, J.-M. Grenèche, N. Menguy, P. Sainctavit and S. Ammar, On the exact crystal structure of exchange-biased Fe3O4–CoO nanoaggregates produced by seed-mediated growth in polyol, *CrystEngComm*, 2016, **18**, 3799–3807.

25 F. Qu, J. Liu, Y. Wang, S. Wen, Y. Chen, X. Li and S. Ruan, Hierarchical Fe3O4@Co3O4 core–shell microspheres: Preparation and acetone sensing properties, *Sens. Actuators, B*, 2014, **199**, 346–353.

Published on 02 February 2026. Downloaded by INIST-CNRS - (Physics) on 3/27/2026 2:38:31 PM.

26 C. V. Schenck, J. G. Dillard and J. W. Murray, Surface analysis and the adsorption of Co(II) on goethite, *J. Colloid Interface Sci.*, 1983, **95**, 398–409.
27 G. Salazar-Alvarez, J. Sort, A. Uheida, M. Muhammed, S. Suriñach, M. D. Baró and J. Nogués, Reversible post-synthesis tuning of the superparamagnetic blocking temperature of γ-Fe $_2O_3$ nanoparticles by adsorption and desorption of Co(ii) ions, *J. Mater. Chem.*, 2007, **17**, 322–328.
28 A. Uheida, G. Salazar-Alvarez, E. Björkman, Z. Yu and M. Muhammed, Fe3O4 and γ-Fe2O3 nanoparticles for the adsorption of Co2+ from aqueous solution, *J. Colloid Interface Sci.*, 2006, **298**, 501–507.
29 L. Fablet, F. Choueikani, M. Pédrot, M. Kerdiles, M. Pasturel and R. Marsac, Investigation of magnetite–Co interactions: from environmentally relevant trace Co levels to core–shell Fe3O4@Co(OH)2 nanoparticles with magnetic applications, *Environ. Sci.: Nano*, 2023, **10**, 3051–3061.
30 G. Ratié, K. Zhang, M. Iqbal, D. Vantelon, F. Mahé, C. Rivard, M. Komárek, M. Bouhnik-Le Coz, A. Dia, K. Hanna, M. Davranche and R. Marsac, Driving forces of Ce(III) oxidation to Ce(IV) onto goethite, *Chem. Geol.*, 2023, **633**, 121547.
31 X. Han, Y.-F. Wang, X.-K. Tang, H.-T. Ren, S.-H. Wu and S.-Y. Jia, Lepidocrocite-catalyzed Mn(II) oxygenation by air and its effect on the oxidation and mobilization of As(III), *Appl. Geochem.*, 2016, **72**, 34–41.
32 E. Demangeat, M. Pédrot, A. Dia, M. Bouhnik-le-Coz, F. Grasset, K. Hanna, M. Kamagate and F. Cabello-Hurtado, Colloidal and chemical stabilities of iron oxide nanoparticles in aqueous solutions: the interplay of structural, chemical and environmental drivers, *Environ. Sci.: Nano*, 2018, **5**, 992–1001.
33 W. B. Fortune and M. G. Mellon, Determination of Iron with o-Phenanthroline: A Spectrophotometric Study, *Ind. Eng. Chem., Anal. Ed.*, 1938, **10**, 60–64.
34 H. Tamura, N. Katayama and R. Furuichi, The Co2+ Adsorption Properties of Al_2O_3, Fe2O3, Fe3O4, TiO2, and MnO_2Evaluated by Modeling with the Frumkin Isotherm, *J. Colloid Interface Sci.*, 1997, **195**, 192–202.
35 K. O. Zahir and H. Keshtkar, A Colorimetric Method for Trace Level Determination of Cobalt in Natural and Waste Water Samples, *Int. J. Environ. Anal. Chem.*, 1998, **72**, 151–162.
36 P. Ohresser, E. Otero, F. Choueikani, K. Chen, S. Stanescu, F. Deschamps, T. Moreno, F. Polack, B. Lagarde, J.-P. Daguerre, F. Marteau, F. Scheurer, L. Joly, J.-P. Kappler, B. Muller, O. Bunau and Ph. Sainctavit, DEIMOS: A beamline dedicated to dichroism measurements in the 350–2500 eV energy range, *Rev. Sci. Instrum.*, 2014, **85**, 013106.
37 V. Briois, C. L. Fontaine, S. Belin, L. Barthe, T. Moreno, V. Pinty, A. Carcy, R. Girardot and E. Fonda, ROCK: the new Quick-EXAFS beamline at SOLEIL, *J. Phys.: Conf. Ser.*, 2016, **712**, 012149.
38 C. Lesage, E. Devers, C. Legens, O. Roudenko, O. Delpoux, A. Beauvois, T. Putaud and V. Briois, Speciation of the Oxide Phase of Molybdenum-Based HDS Catalysts Enhanced with Organic Additives Using an EXAFS/Raman Coupling Methodology, *ChemCatChem*, 2025, **17**, e202401403.
39 G. Landrot, *FASTOSH: a software to process XAFS data for geochemical & environmental applications*, Goldschmidt, Boston, 2018, p. 1402.
40 D. Kinniburgh and D. Cooper, *PhreePlot: Creating graphical output with PHREEQC*.
41 M. W. Haverkort, Thesis, University Koeln, 2005.
42 F. M. F. de Groot, M. Abbate, J. van Elp, G. A. Sawatzky, Y. J. Ma, C. T. Chen and F. Sette, Oxygen 1s and cobalt 2p X-ray absorption of cobalt oxides, *J. Phys.: Condens. Matter*, 1993, **5**, 2277–2288.
43 F. Bosi, U. Hålenius and H. Skogby, Crystal chemistry of the magnetite-ulvöspinel series, *Am. Mineral.*, 2009, **94**, 181–189.
44 T. Sodaee, A. Ghasemi and R. S. Razavi, Controlled growth of large-area arrays of gadolinium-substituted cobalt ferrite nanorods by hydrothermal processing without use of any template, *Ceram. Int.*, 2016, **42**, 17420–17428.
45 X. Liu and C. T. Prewitt, High-temperature X-ray diffraction study of Co3O4: Transition from normal to disordered spinel, *Phys. Chem. Miner.*, 1990, **17**, 168–172.
46 R. Ma, Z. Liu, K. Takada, K. Fukuda, Y. Ebina, Y. Bando and T. Sasaki, Tetrahedral Co(II) Coordination in α-Type Cobalt Hydroxide: Rietveld Refinement and X-ray Absorption Spectroscopy, *Inorg. Chem.*, 2006, **45**, 3964–3969.
47 M. Hall, C. Underwood, T. Failes, G. Foran and T. Hambley, Using XANES to Monitor the Oxidation State of Cobalt Complexes, *Aust. J. Chem.*, 2007, **60**, 180–183.
48 A. Moen, D. G. Nicholson, B. S. Clausen, P. L. Hansen, A. Molenbroek and G. Steffensen, X-ray Absorption Spectroscopic Studies at the Cobalt K-Edge on a Reduced Al_2O_3-Supported Rhenium-Promoted Cobalt Fischer–Tropsch Catalyst, *Chem. Mater.*, 1997, **9**, 1241–1247.
49 A. Moen, D. G. Nicholson, M. Rønning and H. Emerich, In situ X-ray absorption spectroscopic studies at the cobalt K-edge on an Al2O3-supported rhenium-promoted cobalt Fischer-Tropsch catalyst. Comparing reductions in high and low concentration hydrogen, *J. Mater. Chem.*, 1998, **8**, 2533–2539.
50 C. Nordhei, A. L. Ramstad and D. G. Nicholson, Nanophase cobalt, nickel and zinc ferrites: synchrotron XAS study on the crystallite size dependence of metal distribution, *Phys. Chem. Chem. Phys.*, 2008, **10**, 1053–1066.
51 J.-H. Choy, H. Jung and J.-B. Yoon, Co K-edge XAS study on a new cobalt-doped-SiO_2 pillared clay, *J. Synchrotron Radiat.*, 2001, **8**, 599–601.
52 Q. Yang, P. Cui, Q. Ye, S. Chen and Z. Wu, X-ray absorption study of the geometry structure of Co2+/Co3+ in ammonia solution, *J. Mol. Struct.*, 2015, **1098**, 306–310.
53 H. Yan, R. A. Mayanovic, J. Demster and A. J. Anderson, In situ XANES Study of Co2+ Ion Adsorption on Fe3O4 Nanoparticles in Supercritical Aqueous Fluids, *MRS Online Proc. Libr.*, 2012, **1383**, mrsf11.

 This journal is © The Royal Society of Chemistry 2026

54 M. H. Nilsen, C. Nordhei, A. L. Ramstad, D. G. Nicholson, M. Poliakoff and A. Cabañas, XAS (XANES and EXAFS) Investigations of Nanoparticulate Ferrites Synthesized Continuously in Near Critical and Supercritical Water, *J. Phys. Chem. C*, 2007, **111**, 6252–6262.

55 H. L. Andersen, M. Saura-Múzquiz, C. Granados-Miralles, E. Canévet, N. Lock and M. Christensen, Crystalline and magnetic structure–property relationship in spinel ferrite nanoparticles, *Nanoscale*, 2018, **10**, 14902–14914.

Published on 02 February 2026. Downloaded by INIST-CNRS - (Physics) on 3/27/2026 2:38:31 PM.